Bendola Publishing
Journal of Transition Metal Complexes
Vol. 6 (2023), Article ID 246148, 7 pages
doi:10.32371/jtmc/246148

Research Article

Synthesis and Characterization of Nd_2O_3 Nanoparticles Using Urea As Precipitation Agent

Maryam Mohammadi,[1] Bahram Khoshnevisan,[1] and Mohsen Moradian[2]

[1] *Faculty of Physics, University of Kashan, Kashan 87317, Iran*
[2] *Department of Organic Chemistry, Faculty of Chemistry, University of Kashan, Kashan 87317, Iran*
Address correspondence to Bahram Khoshnevisan, b.khosh@kashanu.ac.ir

Received 18 September 2022; Revised 29 December 2022; Accepted 31 December 2022

Abstract Nanoparticles (NPs) of neodymium oxide were prepared by homogeneous co-precipitation method using neodymium nitrate and urea as precursors. X-ray diffraction (XRD) patterns have been refined by the Rietveld method and the Fourier-transform infrared spectroscopy (FT-IR) showed that the sample had a bandgap of about 4.59 eV. On the other hand, the photoluminescence (PL) spectrum indicated that the sample had a low concentration of singly ionized oxygen vacancies. The paramagnetic property of the NPs has been also tested by vibrating-sample magnetometer (VSM) measurements.

Keywords rare earth elements; homogeneous precipitation; urea; Nd_2O_3 NPs; optical properties; Rietveld refinement

1. Introduction

Rare earth elements are strategic resources with widespread use in industry, agriculture, military industry, environmental protection, and medicine. Their compounds are widely utilized in high-performance luminescence devices, magnets, catalysts, display devices, solid-state lasers, and other basic materials due to the electronic, optical, and chemical properties of their 4f-shell ions [1,2,3]. Among them, neodymium-based materials have found their place in various applications and products including magnetic suspensions, photoluminescence (PL), photo materials, magnetic molecules, soft glass, and soft magnets (hexagonal or garnet crystal structure for hard magnets and crystalline structure for soft magnets) [4,5,6,7]. For instance, a well-known material in this category is neodymium oxide, which its optical properties have been associated with applications such as photonics [8], supercapacitor applications [9], luminescent and thermo-luminescent materials [10], protective coatings [11], thin films [12], sensors (e.g., CO and hydrogen gas, etc.) [13]. Since the size and morphology of the particles affect their properties and applications, such as ceramic catalyst applications, scientists are seeking to improve their sensitizing methods (hydrothermal, combustion solution, sol-gel, micro-emulsion, etc.) [14, 15,16,17,18,19,20,21].

It is also important to note that Nd_2O_3 nanoparticles (NPs) have luminescence applications since their bandgap is between 5.25 eV and 5.70 eV and the ability to obtain UV, blue, green, and red luminescence (emission range 200–800 nm) for specific purposes is crucial in optics and luminescence materials [22]. To date, the production of neodymium oxide has employed a wide range of processes, which demand a variety of precursors and commonly involve high temperatures. For example, the synthesis of nanocrystalline Nd_2O_3 through an inductively coupled radiofrequency thermal plasma route could lead to a stable hexagonal crystal structure and the synthesized NPs are highly uniform with an average size of around 20 nm [23]. Another investigation for the synthesis of this NP was designed by Michel et al.; these Nd_2O_3 microspheres were prepared by a solution co-precipitation method for the purpose of gas sensing of CO and CO_2 [9]. The hydrothermal method was employed to first form NdOOH nanorods at 350 °C, followed by the formation of hexagonal NPs of neodymium oxide at 900 °C [24]. After annealing Nd complexes at high temperatures (> 800 °C), hexagonal Nd_2O_3 was obtained [22]. The precipitation of trivalent lanthanide oxides in aqueous solutions is not feasible due to the low hydrolysis tendency of trivalent lanthanide ions in aqueous solutions below pH = 5. It has been shown that homogeneous precipitation of nitrate salts using urea can yield fine NPs [25,26]. Therefore, submicron particles were obtained by decomposing urea in lanthanide salt solutions at high temperatures [27].

Metal (hydrated) oxides with uniform particle size in an aqueous medium have been prepared and were (and are nowadays) a promising topic. Soler-Iltia et al. [26] used this method to synthesize amorphous and crystalline metal (hydrated) oxide. According to their study, ammonia and carbon dioxide are slowly formed in the solution through the decomposition of urea. The smooth pH

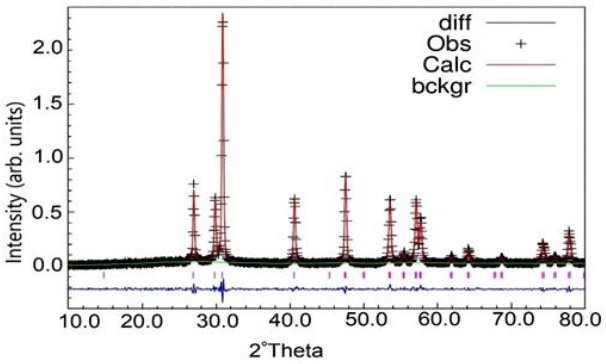

Figure 1: Rietveld refinement of Nd_2O_3.

increase resulting from this degradation at the same time, along with the releasing of OH^- and CO_3^{2-} ions usually leads to the precipitation of metal oxide particles with controlled morphology [28]. In order to make lanthanum oxides, Matijević et al. employed the urea precipitation procedure. By aging at elevated temperatures solutions of corresponding salts in the presence of urea, oxide lanthanide (Gd, Eu, Tb, Sm, Ce) compounds of narrow particle size distribution were produced [27].

In this study, Nd_2O_3 NPs were prepared by homogeneous co-precipitation using urea and their structure, and the NPs were characterized in terms of X-ray diffraction (XRD) Rietveld refinement, morphology, size distribution, and nature of their chemical bonds. The XRD and scanning electron microscopy are used for structural and morphological studies. Fourier transform infrared spectroscopy is used to investigate the nature of existing bonds. The changes in the crystal structure with increasing temperature were evaluated using thermogravimetric analysis (TGA). The optical response of the NPs is investigated through the electronic transition of Nd^{3+} ions in its crystalline structure via the diffuse reflection spectroscopy (DRS) technique. PL was used for studying the presence of defect states and corresponding activation energies in the samples, and to investigate the sample's magnetic properties, vibrating-sample magnetometer (VSM) technique was employed, respectively.

2. Experimental

2.1. Materials

The chemicals used were all analytical reagent grade or chemically pure grade. Neodymium nitrate hexahydrate ($Nd(NO_3)_3 \cdot 6H_2O$) and urea (CH_4N_2O) were purchased from Sigma-Aldrich, (99.9%), and deionized water was used in all procedures.

2.2. Physical measurements

XRD has been employed for structural studies of the synthesized NPs (XRD, Philips-X'Pert Pro, with Cu kα radiation with $\lambda = 1.5405$ Å), and the result was analyzed by Rietveld refinement technique via General Structure Analyze System (GSAS) software. The magnetic properties were studied by a VSM with a maximum field of up to 10 kOe at room temperature. The morphology and microstructure of the sample were observed with a Field Emission Scanning Electron Microscope (FESEM) (TESCAN BRNO-Mira3 LMU), and energy dispersive X-ray (EDX) analysis was used for testing elemental composition (at an accelerating voltage of 20 kV). IR spectrum was recorded with a KBr pellet on a Perkin-Elmer 781 spectrophotometer. The PL studies have been carried out using a Perkin-Elmer LS-55 luminescence spectrophotometer equipped with an Xe lamp. The UV-Vis absorption spectra were recorded by a DRS method (Shimadzu, UV-1800, Japan) to calculate the bandgap of the sample. TGA was carried out with a STA1500 (Rheometric Scientific) instrument at a heating rate of 10 °C min^{-1} under air atmosphere.

Table 1: Rietveld refinement results for Nd_2O_3.

A	Oxidation state	x	y	z	Occupancy
Nd1	+3	0.333301	0.666700	0.240802	1
Nd2	+3	0.666600	0.333299	0.747891	1
O1	−2	0.000000	0.000000	0.034332	1
O2	−2	0.333301	0.666700	0.633250	1
O3	−2	0.666600	0.333299	0.346650	1

Space group: p3m1 (164) $a = b = 3.8302$ Å, $c = 6.0002$ Å, $R_p = 0.0751$, $wR_p = 0.1138$, $\chi^2 = 0.87$.

2.3. Synthesis

To make the neodymium oxide NPs, according to the literature with some modification [28], first 0.05 g (0.11 mmol) of $Nd(NO_3)_3 \cdot 6H_2O$, 0.5 g (8.3 mmol) of urea (CH_4N_2O) was dissolved in 40 mL of DI water, then the solution was sonicated for 30 min. The mixtures were heated to 90 °C and maintained for 3–4 h for sedimentation. This sediment was calcinated for 3 h in the furnace at 800 °C to obtain Nd_2O_3 NPs. The chemical process would be along with the following relation:

$$2Nd(NO_3)_3 + 5CH_4N_2O \rightarrow Nd_2O_3 + 5CO_2 + 8N_2 + 10H_2O.$$

3. Results and discussion

The phase and crystal structure of the prepared Nd_2O_3 NPs by the homogenous urea co-precipitation method was examined by Rietveld refinements of the XRD pattern which is a unique and comprehensive method for estimating an approximate structural model for the real structure [29, 30]. The refined profile is shown in Figure 1, and some of the refined structural parameters like atomic site occupancy and the relative position of the atoms in the unit cell (x, y, z) are listed in Table 1.

The diffraction peaks in the XRD pattern of the Nd_2O_3 NPs at 2θ = 26.8 °C, 29.7 °C, 30.7 °C, 40.5 °C, 47.4 °C,

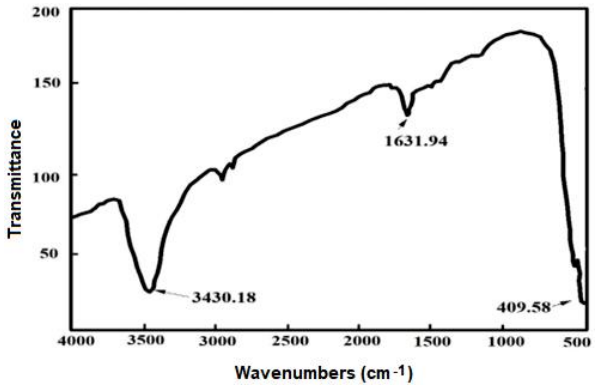

Figure 2: FTIR spectra of Nd_2O_3 NPs.

53.4 °C, 56.2 °C, 57.6 °C, and 77.7 °C are related to (100), (002), (011), (012), (110), (103), (112), (201), and (121) respectively corresponding to the standard pattern reference of Nd_2O_3 (JCPDS Card No. 074-2139) [31,32]. The structure was hexagonal and the difference curve indicated a significant confirmation between the calculated and the collected XRD pattern. The lattice parameter values were $a = b = 3.8302$ Å and $c = 6.0002$ Å; the cell volume was 77.68 Å^3; and the NPs were well crystallized with very high purity which is in good agreement with the literature [33]. By using Debye–Scherrer's equation:

$$D = \mathrm{k}\lambda/\beta\cos\theta,$$

where k = 0.89 is a constant, θ is Bragg's angle, and β is full width at half maximum (FWHM) of the peaks [34]; the average size of the nanocrystals was ~ 30 nm.

Fourier-transform infrared (FT-IR) spectra were used to reveal the chemical structure of the fabricated Nd_2O_3 NPs, which is displayed in Figure 2.

Based on the chosen colloidal system, aqueous media are adjusted to pH levels between 5 and 6. In the construction process of Nd_2O_3 NPs, urea reacts with water above 70 °C and ammonia, hydroxide, and carbonate ions (carbon dioxide), which causes the pH reach to 9 during the aging period in about 1–2 h at 85 °C, according to the equation below:

$$(H_2N_2)_2CO + 3\,H_2O \rightarrow CO_2 + 2\,NH_4^+ + 2\,OH^-.$$

Therefore, $Nd(OH)_3$ is precipitated by $Nd(NO_3)_3$ in the presence of ammonia, which upon further heat treatment transformed into neodymium oxide [27]. In the FTIR spectrum of Nd_2O_3 NPs, the absorption peak at 409.58 cm^{-1} indicated Nd−O bond stretching vibrations [35].

The absorption bands at 1631 cm^{-1} and 3430 cm^{-1} are assigned to the stretching and bending vibrations of water molecules absorbed by Nd_2O_3 NPs, respectively [27]. It was suggested that water with carbonate ions had intermolecular H bonds between 2,500 cm^{-1} and 3,000 cm^{-1} [36].

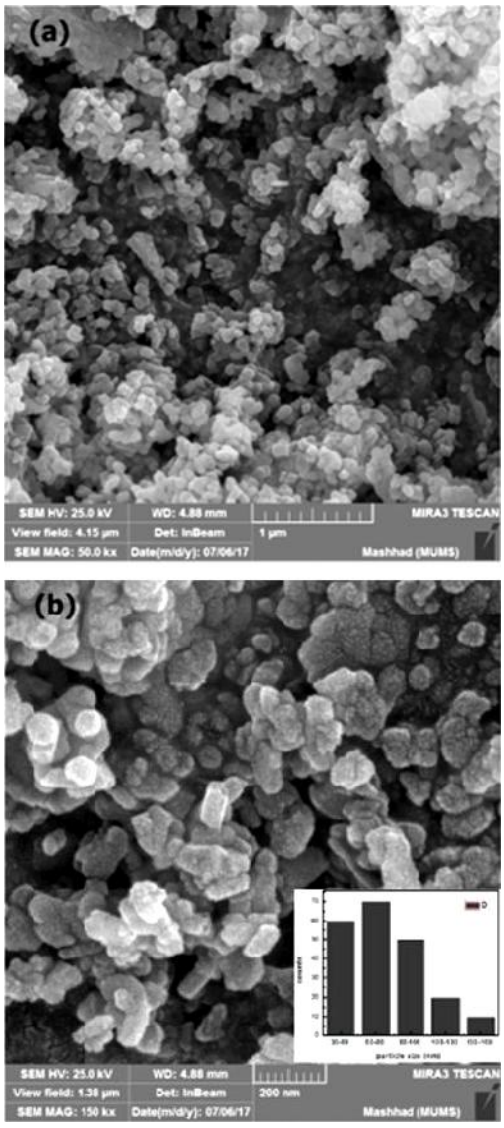

Figure 3: FESEM morphology of Nd_2O_3 calcinated at 800 °C (a) 1 μm (b) 200 nm and size abundance distribution of NPs.

Figure 3 shows the surface morphology of the Nd_2O_3 NPs as formed and heat-treated at 800 °C for 3 h and its fractional NPs size range is also obtained. The average size of NPs is between 60 nm and 80 nm. The FESEM study of NPs at two different scales (1 μm and 200 nm) revealed that NPs are spherical, amorphous, and agglomerated [37]. These data indicate that the observed NPs from the FESEM image consist of several interconnected crystallines.

An EDX analysis was performed to evaluate the presence of elements in the sample (Figure 4). This technique provides an overall map of the sample by analyzing the elements near the surface and estimating the proportion of different elements at different locations on the surface. There are two elements that can be seen in the EDX spectrum,

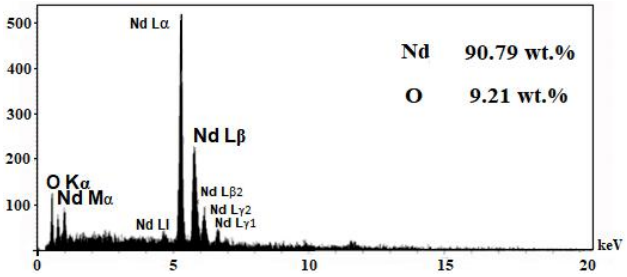

Figure 4: EDX result of Nd_2O_3 NPs.

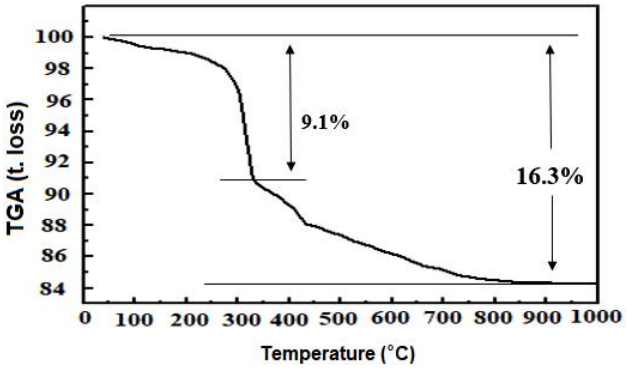

Figure 5: Typical TGA analysis curves of the Nd_2O_3 sample.

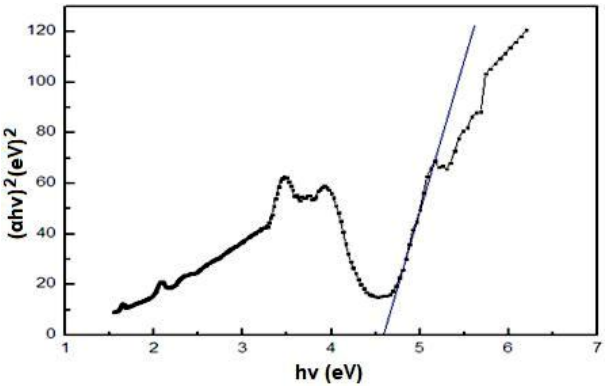

Figure 6: Band gap of Nd_2O_3 NPs.

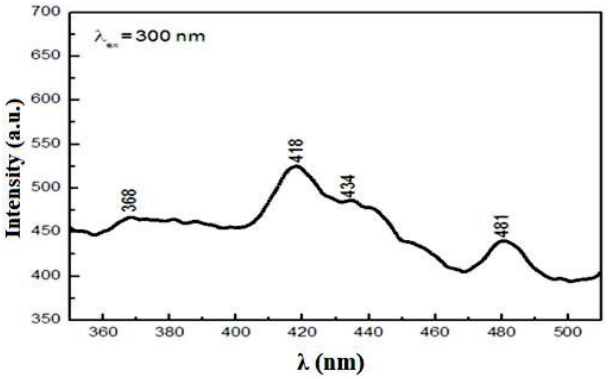

Figure 7: PL spectrum of the Nd_2O_3 NPs in the range of 340–520 nm.

Nd, and O. It is confirmed from the XRD, FT-IR, and EDX analysis that neodymium oxide NPs are constructed [38].

The TGA can provide useful information about the sample, respectively (Figure 5). As the sample is heated, it may undergo various reactions such as reduction, oxidation, evaporation, water/CO_2 adsorption or desorption, phase transformation, etc. This process can be evaluated to determine how the physical and chemical properties of the sample change. During a heated period of 260 °C to 340 °C, a rigid weight loss of about 9.1% was observed. The endothermic peak at around 330 °C indicates a change in the crystal structure which may be due to the first dehydration process ($2Nd(OH)_3 \rightarrow 2NdOOH + 2H_2O$). It is determined from the obtained TGA curves that a total weight loss of 16.3% is observed for NPs. As indicated by the XRD pattern, the second hydration process occurs at a temperature of 800 °C ($2Nd(OH)_3 \rightarrow Nd_2O_3 + 3H_2O$) [24, 39].

Figure 6 displays the diffuse reflection spectroscopy (DRS) technique for investigating the optical property of the Nd_2O_3 NPs calcined at 800 °C for 3 h and exhibits an adsorption band with a maximum at 272 nm. Nanomaterials tend to have a higher surface-to-volume ratio than bulk counterparts, which leads to more defects on the surface. Therefore, nanomaterials with small particle size exhibit strong and broad absorption bands. For the synthesized Nd_2O_3 NPs consequently, defects are more likely to be distributed on the surface, as well [40].

The optical energy band gaps E_g of the nano- and microcrystalline materials are calculated by using the Tauc relation [41,42]:

$$(\alpha h\nu)^2 = A(h\nu - E_g),$$

where α is the optical absorption coefficient near the fundamental absorption edge. The bandgap is obtained from the intersection of the tangential slope of the high energy range of the DRS spectra and the horizontal axis (Figure 6).

The energy band gap of these NPs is about 4.59 eV and indicated that the Nd_2O_3 sample might be employed as a photocatalyst under ultraviolet light [32,40].

The complementary study of the emission property of NPs has been done by PL spectroscopy and the spectrum was scanned in the wide wavelength range of 200 nm ∼ 800 nm. The excitation wavelengths were 300 nm, 340 nm, and 380 nm. Figure 7 is the PL spectrum in relation to the photo excited wavelength of 300 nm and the observed weak peaks at ∼ 368–398 nm (UV) could be attributed to singly ionized oxygen vacancies in the Nd_2O_3 NPs (by the radiative recombination of photo-generated holes and electron occupying the oxygen vacancies [35]). It is worth

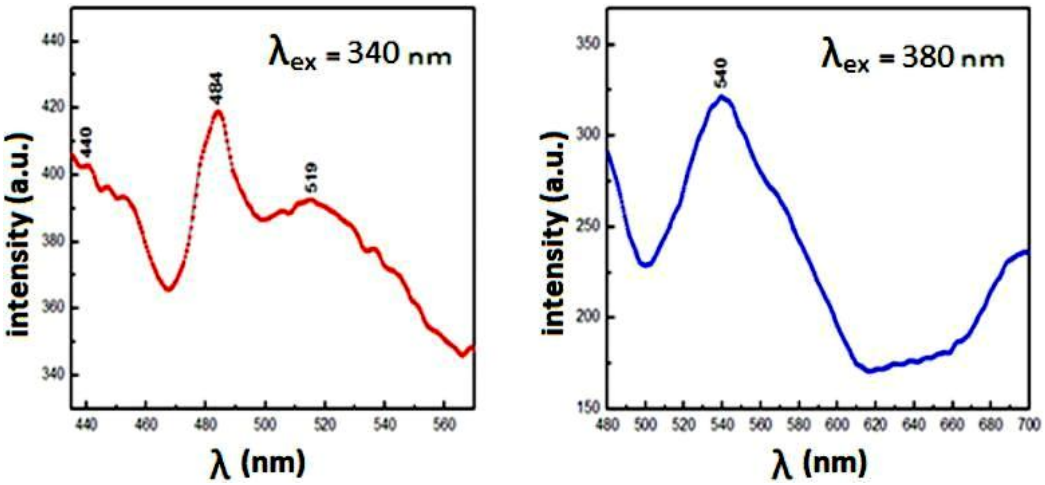

Figure 8: PL spectrum of the Nd_2O_3 NPs in the range of 430–580 nm and 480–700 nm.

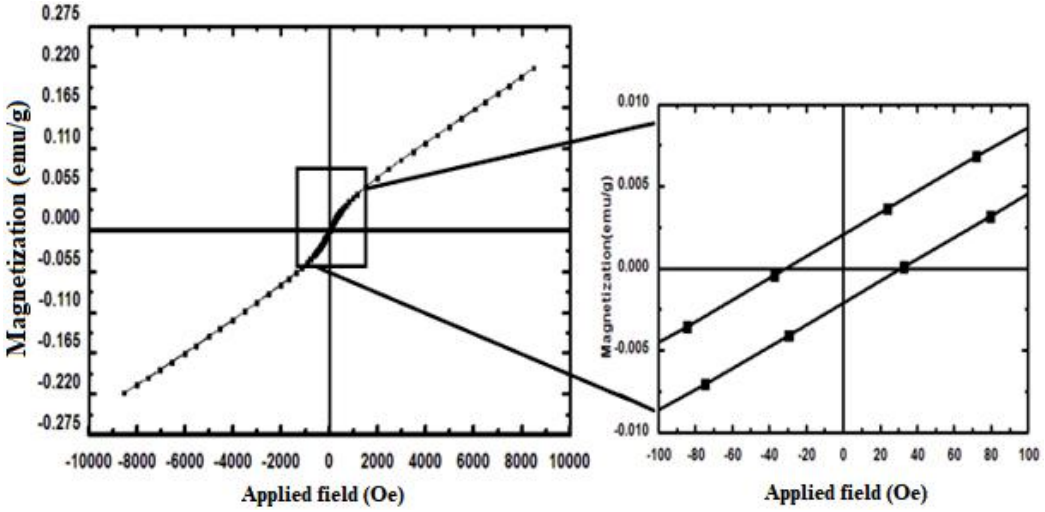

Figure 9: VSM of Nd_2O_3 NPs at room temperature.

noting that the relatively low intensity of the PL spectrum in this range (compared to the literature) means that the sample had a low concentration of singly ionized oxygen vacancies via this fabrication method. Moreover, the emission spectra also exhibit a series of emission peaks with maxima at 418–481 nm (blue). The PL peak 340 nm excitation shows a series of emission peaks with the maximum at 440–484 nm (blue) and 519 nm (green), and also the 380 nm excitation wavelength shows a maximum peak at 540 nm (green) (Figures 7 and 8). In general, the UV, blue, and green emissions exhibited the presence of surface defects and recombination of electrons by shallow defect levels exciting holes in the valence band. The blue and green emissions are presumably due to surface defects such as Schottky and Frankel in the lattice. In addition, they indicated that the fabricated Nd_2O_3 NPs are a promising candidate for optical and biomedical applications because the blue and the green emission bands resulted from $({}^4I_{9/2} \rightarrow {}^2P_{3/2}, {}^2K_{15/2})$ and $({}^4I_{9/2} \rightarrow {}^4G_{5/2}, {}^4G_{7/2})$ transitions, respectively [43].

For the investigation of the magnetic properties of the sample, we have employed VSM measurement and M–H loop shows a nonlinear hysteretic nature (Figure 9). The coercivity magnitude of these NPs was about 23.29 Oe. The magnetization with the applied field indicates an unsaturated M–H loop in high field region even at a maximum applied field of 10 kOe. Due to the high free ion magnetic moment of Nd^{3+}, the paramagnetic behavior of Nd_2O_3 starts to dominate ferromagnetic behavior above 600 Oe [44].

4. Conclusions

In this study, the synthesis of Nd_2O_3 NPs by using the urea co-precipitation method was investigated, which was confirmed by Rietveld refinements of the XRD pattern with the lattice parameters of $a = b = 3.8302$ Å and $c = 6.0002$ Å;

volume cell 77.68 Å^3; and space group of p3m1. SEM image shows that the NPs were spherical, amorphous, and agglomerated and their average size was in the range of 60–80 nm. The energy gap of the NPs was obtained using the DRS analysis ($\sim$ 4.59 eV). The PL spectra of these NPs were investigated with excitation wavelengths of 300 nm, 340 nm, and 380 nm. At the excitation of 300 nm, the NPs exhibited a series of emission peaks with maxima at 418–481 nm (blue). The 340 nm excitation wavelength shows a series of emission peaks with the maximum at 440–484 nm (blue) and 519 nm (green), and also the 380 nm excitation wavelength showed a peak at 540 nm (green). By the VSM examination of the magnetic properties of these NPs, it was found that the sample is paramagnetic that arising from the high free ion magnetic moment of Nd^{3+}.

Conflict of interest The authors declare that they have no conflict of interest.

References

[1] X. Qu, J. Dai, J. Tian, et al., *Syntheses of Nd_2O_3 nanowires through sol-gel process assisted with porous anodic aluminum oxide (AAO) template*, J Alloys Compd, 469 (2009), 332–335.

[2] L. Qian, Y. Gui, S. Guo, Q. Gong, and X. Qian, *Controlled synthesis of light rare-earth hydroxide nanorods via a simple solution route*, J Phys Chem Solids, 70 (2009), 688–693.

[3] R. Bazzi, M. A. Flores-Gonzalez, C. Louis, et al., *Synthesis and luminescent properties of sub-5-nm lanthanide oxides nanoparticles*, J Lumin, 102-103 (2003), 445–450.

[4] W. Que, C. H. Kam, Y. Zhou, Y. L. Lam, and Y. C. Chan, *Yellow-to-violet upconversion in neodymium oxide nanocrystal/titania/ormosil composite sol-gel thin films derived at low temperature*, J Appl Phys, 90 (2001), 4865–4867.

[5] K. T. Kubra, R. Sharif, B. Patil, et al., *Hydrothermal synthesis of neodymium oxide nanoparticles and its nanocomposites with manganese oxide as electrode materials for supercapacitor application*, J Alloys Compd, 815 (2020), 152104.

[6] B. Umesh, B. Eraiah, H. Nagabhushana, et al., *Structural characterization, thermoluminescence and EPR studies of Nd_2O_3:Co^{2+} nanophosphors*, Mater Res Bull, 48 (2013), 180–187.

[7] S. Chevalier, G. Bonnet, and J. P. Larpin, *Metal-organic chemical vapor deposition of Cr_2O_3 and Nd_2O_3 coatings. Oxide growth kinetics and characterization*, Appl Surf Sci, 167 (2000), 125–133.

[8] R. Sarma, D. Saikia, P. Saikia, P. K. Saikia, and B. Baishya, *Pentacene based thin film transistors with high-k dielectric Nd_2O_3 as a gate insulator*, Braz J Phys, 40 (2010), 357–360.

[9] C. R. Michel, A. H. Martínez-Preciado, and N. L. L. Contreras, *Gas sensing properties of Nd_2O_3 nanostructured microspheres*, Sens Actuators B Chem, 184 (2013), 8–14.

[10] R. E. Riman, G. A. Kumar, V. Atakan, J. G. Brennan, and J. Ballato, *Engineered solution synthesis of rare-earth nanomaterials and their optical properties*, in Penetrating Radiation Systems and Applications VIII, F. P. Doty, H. B. Barber, and H. Roehrig, eds., vol. 6707, SPIE, Bellingham, WA, 2007, 69–79.

[11] J. McKittrick, L. E. Shea, C. F. Bacalski, and E. J. Bosze, *The influence of processing parameters on luminescent oxides produced by combustion synthesis*, Displays, 19 (1999), 169–172.

[12] Y.-P. Fu, S.-B. Wen, and C.-S. Hsu, *Preparation and characterization of $Y_3Al_5O_{12}$:Ce and Y_2O_3:Eu phosphors powders by combustion process*, J Alloys Compd, 458 (2008), 318–322.

[13] G. Jia, K. Liu, Y. Zheng, Y. Song, M. Yang, and H. You, *Highly uniform $Gd(OH)_3$ and Gd_2O_3:Eu^{3+} nanotubes: facile synthesis and luminescence properties*, J Phys Chem C, 113 (2009), 6050–6055.

[14] L. Kępiński, M. Zawadzki, and W. Mišta, *Hydrothermal synthesis of precursors of neodymium oxide nanoparticles*, Solid State Sci, 6 (2004), 1327–1336.

[15] B. A. A. Balboul and A. Y. Z. Myhoub, *The characterization of the formation course of neodymium oxide from different precursors: A study of thermal decomposition and combustion processes*, J Anal Appl Pyrolysis, 89 (2010), 95–101.

[16] T. Sreethawong, S. Chavadej, S. Ngamsinlapasathian, and S. Yoshikawa, *Sol-gel synthesis of mesoporous assembly of Nd_2O_3 nanocrystals with the aid of structure-directing surfactant*, Solid State Sci, 10 (2008), 20–25.

[17] R. Jian-Hua, Z. Tong-Gang, L. Jian-Hua, K. Juan, H. Jia-Xin, and G. Lin, *Synthesis and photoluminescence properties of Nd_2O_3 nanoparticles modified by sodium bis(2-ethylhexyl) sulfosuccinate*, Chinese Phys B, 17 (2008), 4669.

[18] A. S. Das, M. Roy, D. Roy, S. Bhattacharya, and P. M. G. Nambissan, *Defects characterization and study of amorphous phase formation in xV_2O_5-(1-x)Nd_2O_3 binary glass nanocomposites using positron annihilation and correlated experimental techniques*, J Alloys Compd, 753 (2018), 748–760.

[19] T. Liu, Y. Zhang, H. Shao, and X. Li, *Synthesis and characteristics of Sm_2O_3 and Nd_2O_3 nanoparticles*, Langmuir, 19 (2003), 7569–7572.

[20] W. Zhu, J. Ma, L. Xu, W. Zhang, and Y. Chen, *Controlled synthesis of $Nd(OH)_3$ and Nd_2O_3 nanoparticles by microemulsion method*, Mater Chem Phys, 122 (2010), 362–367.

[21] P. Wu, Z. Zhang, and G. Song, *Preparation of Nd_2O_3 nanorods in SDBS micelle system*, J Rare Earths, 32 (2014), 1027–1031.

[22] Q. Liqin, W. Kaituo, W. Xuehang, W. Wenwei, L. Sen, and L. Gengming, *Nanocrystalline Nd_2O_3: Preparation, phase evolution, and kinetics of thermal decomposition of precursor*, Ceram Int, 40 (2014), 3003–3009.

[23] S. Sohn, Y. Kwon, Y. Kim, and D. Kim, *Synthesis and characterization of near-monodisperse yttria particles by homogeneous precipitation method*, Powder Technol, 142 (2004), 136–153.

[24] S. H. Jeon, K. Nam, H. J. Yoon, Y.-I. Kim, D. W. Cho, and Y. Sohn, *Hydrothermal synthesis of Nd_2O_3 nanorods*, Ceram Int, 43 (2017), 1193–1199.

[25] A. Ookubo, K. Ooi, and T. Tomita, *New types of hydrous titanium oxides obtained by homogeneous precipitation from (titanium (III) chloride + urea) solutions*, J Mater Sci, 24 (1989), 3599–3604.

[26] G. J. Soler-Iltia, M. Jobbagy, R. J. Candal, A. E. Regazzoni, and M. A. Blesa, *Synthesis of metal oxide particles from aqueous media: the homogeneous alkalin1zat1on method*, J Dispers Sci Technol, 19 (1998), 207–228.

[27] E. Matijević and W. P. Hsu, *Preparation and properties of monodispersed colloidal particles of lanthanide compounds: I. Gadolinium, europium, terbium, samarium, and cerium(III)*, J Colloid Interface Sci, 118 (1987), 506–523.

[28] Y. Li, Y. Zhang, G. Hong, and Y. Yu, *Upconversion luminescence of Y_2O_3:Er^{3+}, Yb^{3+} nanoparticles prepared by a homogeneous precipitation method*, J Rare Earths, 26 (2008), 450–454.

[29] B. H. Toby, *EXPGUI, a graphical user interface for GSAS*, J Appl Cryst, 34 (2001), 210–213.

[30] S. C. Vogel, *gsaslanguage: a GSAS script language for automated Rietveld refinements of diffraction data*, J Appl Cryst, 44 (2011), 873–877.

[31] R. Boulesteix, A. Maître, J.-F. Baumard, et al., *The effect of silica doping on neodymium diffusion in yttrium aluminum garnet ceramics: implications for sintering mechanisms*, J Eur Ceram Soc, 29 (2009), 2517–2526.

[32] T. Munawar, F. Mukhtar, M. S. Nadeem, et al., *Novel direct dual-Z-scheme ZnO-Er_2O_3-Nd_2O_3@reduced graphene oxide heterostructured nanocomposite: Synthesis, characterization and superior antibacterial and photocatalytic activity*, Mater Chem Phys, 253 (2020), 123249.

[33] B. Umesh, B. Eraiah, H. Nagabhushana, et al., *Synthesis and characterization of spherical and rod like nanocrystalline Nd_2O_3 phosphors*, J Alloys Compd, 509 (2011), 1146–1151.

[34] P. Goel, N. Vijayan, and A. M. Biradar, *Complex impedance studies of low temperature synthesized fine grain PZT/CeO_2 nanocomposites*, Ceram Int, 38 (2012), 3047–3055.

[35] R. Yuvakkumar and S. I. Hong, *Nd_2O_3: novel synthesis and characterization*, J Sol-Gel Sci Technol, 73 (2015), 511–517.

[36] B. Aiken, W. P. Hsu, and E. Matijević, *Preparation and properties of monodispersed colloidal particles of lanthanide compounds: III, yttrium(III) and mixed yttrium(III)/cerium(III) systems*, J Am Ceram Soc, 71 (1988), 845–853.

[37] S. Rahmatinejad and H. Naeimi, *Graphitic carbon nitride supported neodymium oxide as an efficient recyclable nanocatalyst for the one-pot synthesis of diazabenzo[a]anthraceneones*, Dalton Trans, 51 (2022), 1163–1174.

[38] R. B. Yu, K. H. Yu, W. Wei, et al., *Nd_2O_3 nanoparticles modified with a silane-coupling agent as a liquid laser medium*, Adv Mater, 19 (2007), 838–842.

[39] G. D. Dhamale, V. L. Mathe, S. V. Bhoraskar, S. N. Sahasrabudhe, and S. Ghorui, *Synthesis and characterization of Nd_2O_3 nanoparticles in a radiofrequency thermal plasma reactor*, Nanotechnology, 27 (2016), 085603.

[40] A. Emeline, G. V. Kataeva, A. S. Litke, A. V. Rudakova, V. K. Ryabchuk, and N. Serpone, *Spectroscopic and photoluminescence studies of a wide band gap insulating material: powdered and colloidal ZrO_2 sols*, Langmuir, 14 (1998), 5011–5022.

[41] J. I. Pankove, *Optical Processes in Semiconductors*, Dover Publications, New York, 1971.

[42] J. Tauc, R. Grigorovici, and A. Vancu, *Optical properties and electronic structure of amorphous germanium*, Phys Status Solidi B, 15 (1966), 627–637.

[43] P. Goel and M. Arora, *Mechanism of photoluminescence enhancement and quenching in Nd_2O_3 nanoparticles-ferroelectric liquid crystal nanocomposites*, RSC Adv, 5 (2015), 14974–14981.

[44] B. J. Sarkar, J. Mandal, M. Dalal, A. Bandyopadhyay, and P. K. Chakrabarti, *Room temperature ferromagnetism of nanocrystalline $Nd_{1.90}Ni_{0.10}O_{3-\delta}$*, Appl Phys A, 124 (2018), Article No. 393.